Supporting Information

Compromise and Synergy in Thermoelectric GeTe–$CuSbS_2$ Alloys

Zi-Wei Feng,‡ [a] Meng Li,‡ [b] Yongqi Chen,[b] Siqi Liu,[b] De-Zhuang Wang,[a] Liang-Cao Yin,[a] Hao Wu,[a] Wei-Di Liu,[b] Xiao-Lei Shi,[b] Yifeng Wang,[c] Zhi-Gang Chen, [b,] Qingfeng Liu [a,*]*

[a] State Key Laboratory of Materials-Oriented Chemical Engineering, College of Chemical Engineering, Nanjing Tech University, Nanjing 211816, China.

[b] School of Chemistry and Physics, ARC Research Hub in Zero-emission Power Generation for Carbon Neutrality, and Centre for Materials Science, Queensland University of Technology, Brisbane, Queensland 4000, Australia.

[c] College of Materials Science and Engineering, Nanjing Tech University, Nanjing 211816, China

‡ These authors contributed equally to this work.

* Corresponding authors. E-mail: zhigang.chen@qut.edu.au (Z.-G. Chen), qfliu@njtech.edu.cn (Q. Liu).

1.Experiment details

1.1 Material Synthesis: Raw elements in trace-metal purities, namely Ge (99.99%), Te (99.99%), Cu (99.99%), Sb (99.99%), and S (99.99%), were weighed based on the nominal compositions of GeTe–xCuSbS$_2$ (x=0, 2, 4, 6, 8, 10, 12, 20, 30 mol%). The reagents were sealed in the evacuated quartz tubes, slowly heated up to 1223 K over 12 h in a muffle furnace, soaked at this temperature for 10 h, and followed by quenching in iced water. Subsequently, the attained ingots were annealed at 923 K for 3 days, before being ground into fine powder and sintered by spark plasma sintering (LABOX-110H Sinter Land) under a uniaxial pressure of 50 MPa at 823 K for 5 min in vacuum. The as-fabricated highly dense round disks with a dimension of 12.7 mm were used for property measurement.

1.2 Characterization: Room temperature X-ray diffraction (XRD, Rigaku Smartlab) was performed to analyze the phase purities and crystal structures. Scanning electron microscopy (SEM, Hitachi TM3000) equipped with an energy-dispersive X-ray spectroscopy (EDS) detector and transmission electron microscopy (TEM, FEI Talos F200) were used to investigate the microstructures, lattice structures and compositions. The TEM lamella specimen was prepared using focused ion beam (FIB, FEI Scios). X-ray photoelectron spectroscopy (XPS, Thermo ESCALAB 250) was performed to study the valence states of the samples. The XANES and EXAFS spectra were measured at the XAS beamline in the Australian Synchrotron, and the data was post-processed using the Demeter package.

1.3 Thermoelectric Performance Measurement: Temperature-dependent electrical conductivity (σ) and Seebeck coefficient (S) were measured using a four probe method (SBA 458, NETZSCH) under a protective atmosphere of Argon. Thermal conductivity (κ) was calculated based on $\kappa = \rho C_p D$, where the density (ρ) was determined by the Archimedes method, and the heat capacity (C_p) values were calculated by the Dulong-Petit's law,[1] and the thermal diffusivity (D) was measured by a laser flash method (LFA 457, NETZSCH). The Hall coefficient (R_H) values were measured by the Van der Pauw method with a magnetic field up to ±1.5 T at room temperature. Carrier concentration (n) and mobility (μ) were calculated using $n = 1/(eR_H)$ and $\mu = \sigma R_H$, respectively, where

e represents the electron charge.

1.4 Density Functional Theory (DFT) Calculations: First-principle calculations were performed based on density-functional theory (DFT) with all electron projected augmented wave (PAW) method, as implemented in the Vienna Ab initio Simulation Package (VASP).[2-7] Semi-local generalized gradient approximation (GGA) with the fully relativistic Perdew-Burke-Ernzerhof (PBE) exchange correlation functional was employed.[8] The alloys, based on 3×3×3 supercells, are simulated via the evolutionary algorithm implemented in USPEX, which are sampled by a Monkhorst-Pack **k**-mesh spanning less than 0.03/Å^3 for structural relaxation, and a denser **k**-mesh spanning less than 0.015/Å^3 for non-self-consistencies. The wave functions were expanded in a plan-wave basis with a cut-off energy of 450 eV. All atoms were allowed to relax in their geometric optimizations until the Hellmann–Feynman force is less than 0.01 eV·Å^{-1}, and the convergence criterion for the electronic self-consistent loop was set to 1×10^{-7} eV. The electronic band structures were calculated along the line-mode **k**-path based on Brillouin path features indicated by the AFLOW framework.[9] Spin-orbital coupling (SOC) was considered because Te is a heavy element.

1.5 Debye-Callaway model: Based on the Debye-Callaway model,[10, 11] the lattice thermal conductivity (κ_l) is expressed by

$$\kappa_l = \frac{k_B}{2\pi^2 v}\left(\frac{k_B T}{\hbar}\right)^3 \int_0^{\frac{\theta_D}{T}} \tau_{tot} \frac{z^4 \exp(z)}{[\exp(z)-1]^2} dz \quad \text{(S1)}$$

The integrand item, in conjunction with the coefficient of the above equation is the spectral lattice thermal conductivity (κ_s), namely

$$\kappa_S = \frac{k_B}{2\pi^2 v}\left(\frac{k_B T}{\hbar}\right)^3 \tau_{tot} \frac{z^4 \exp(z)}{[\exp(z)-1]^2} \quad \text{(S2)}$$

In the above equations, v_s is the sound velocity, $\hbar$ is the reduced Plank constant, θ_D is the Debye temperature, τ_{tot} is the total relaxation time, $z = \frac{\hbar\omega}{k_B T}$ (with ω denoting phonon frequency) is the reduced phonon frequency. τ_{tot} is a reciprocal sum of the relaxation times of the pertinent scattering mechanisms.

The phonon scattering pathways generally include phonon-phonon Umklapp scattering (U), grain boundary (B), stacking fault (SF), point defect (PD), and dislocation (D). Thus, τ_{tot} can be calculated by

$$\tau_{tot}^{-1} = \tau_{U}^{-1} + \tau_{B}^{-1} + \tau_{PD}^{-1} + \tau_{SF}^{-1} + \tau_{NP}^{-1} + \tau_{RS}^{-1} \quad \text{(S3)}$$

with relevant phonon relaxation times being:

Umklapp process

$$\tau_{U}^{-1} = \frac{\hbar\gamma^2}{\bar{M}v_s^2\theta_D}\omega^2 T\exp\left(-\frac{\theta_D}{3T}\right) \quad \text{(S4)}$$

Grain boundary scattering

$$\tau_{B}^{-1} = \frac{v_s}{d} \quad \text{(S5)}$$

Point defect scattering

$$\tau_{PD}^{-1} = \frac{\bar{V}\omega^4}{4\pi v_s^3 \Gamma} \quad \text{(S6)}$$

Stacking fault scattering[12, 13]

$$\tau_{SF}^{-1} = 0.7\frac{a^2\gamma^2 N_s}{v_s}\omega^2 \quad \text{(S7)}$$

Nanoprecipitates scattering

$$\tau_{NP}^{-1} = v\left[(2\pi R)^{-1} + \left(\pi R^2\frac{4}{9}\left(\frac{\Delta D}{D}\right)^2\left(\frac{\omega R}{v}\right)^4\right)^1\right]^1 N_p \quad \text{(S8)}$$

Resonant scattering

$$\tau_{RS}^{-1} = \frac{c_i\omega^2}{\left(\omega_i^2 - \omega^2\right)^2} \quad \text{(S9)}$$

In these equations, γ is the Grüneisen parameter, υ is the Poison ratio, $\bar{V}$ is the average atomic volume, $\bar{M}$ is the average atomic mass, Γ is the point defect scattering parameter, a is the refined lattice parameters of sample,d is the grain size, R is the average precipitate radius, D is the matrix density, ΔD is the density difference between the precipitate and matrix, N_p is the number density of precipitates, N_s is the number of SF per unit length, and ω is the frequency of the Einstein oscillator.

2.Supplementary Figures

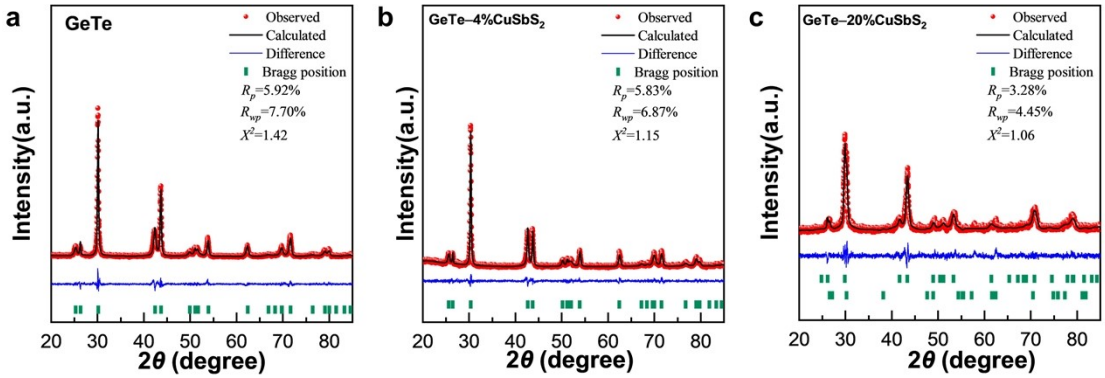

Figure S1. (a-c) The Rietveld refined XRD patterns of x=0, x=4% and x=20% samples.

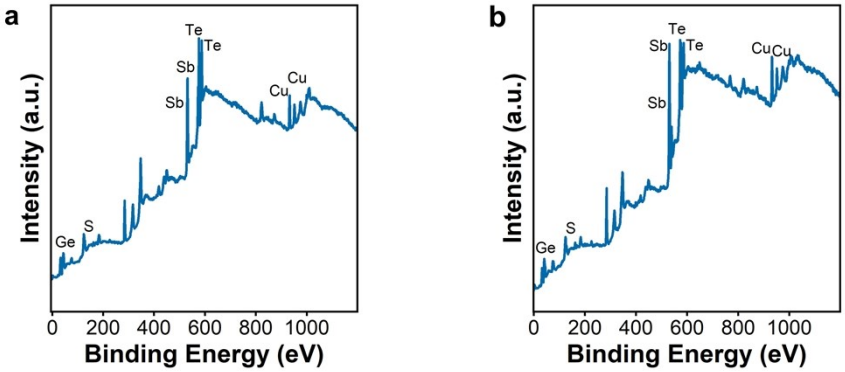

Figure S2. (a-b) XPS full spectrum of x=4% and x=20% samples.

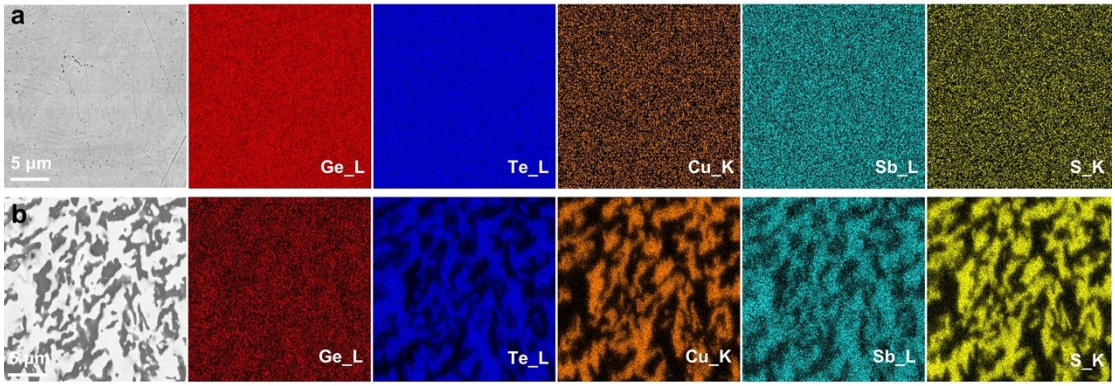

Figure S3. (a-b) BSE image and SEM-EDS elemental mapping of x=4% and 20% samples.

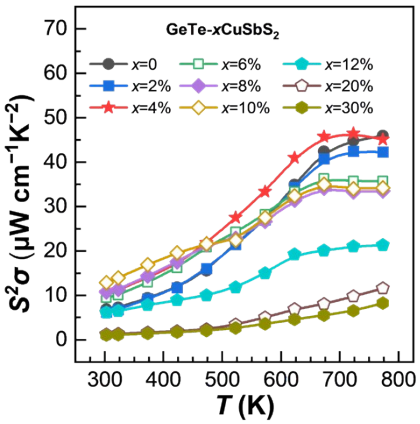

Figure S4. Power factor ($S^2\sigma$) of all samples.

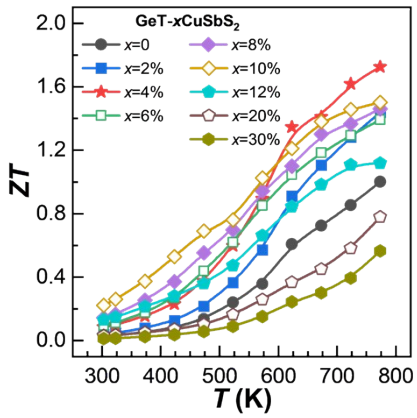

Figure S5. Temperature-dependent ZT of all samples.

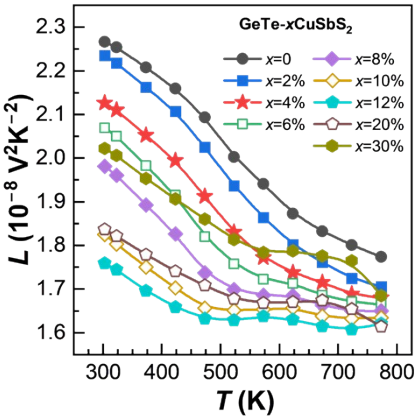

Figure S6. Temperature-dependent Lorenz constant (L) of all samples.

Table S1. Room-temperature density of GeTe-x$CuSbS_2$ (x=2, 4, 6, 8, 10, 12, 20, 30%) samples.

Sample	Dry Weight (g)	Wet Weight (g)	Temperature of Alcohol (℃)	Density of Alcohol (g/cm^3)	Density of Sample (g/cm^3)
GeTe–2%$CuSbS_2$	0.8772	0.7657	26	0.78437	6.1708
GeTe–4%$CuSbS_2$	0.9864	0.8604	26	0.78437	6.1405
GeTe–6%$CuSbS_2$	1.0233	0.8926	26	0.78437	6.1411
GeTe–8%$CuSbS_2$	1.0583	0.9236	26	0.78437	6.1626
GeTe–10%$CuSbS_2$	1.2576	1.1016	26	0.78437	6.3232
GeTe–12%$CuSbS_2$	1.1463	0.9931	29	0.78182	5.8499
GeTe–20%$CuSbS_2$	1.188	1.0256	29	0.78182	5.7192
GeTe–30%$CuSbS_2$	1.1436	0.7963	29	0.78182	2.5744

References

1. B. Qin, D. Wang, W. He, Y. Zhang, H. Wu, S. J. Pennycook and L. D. Zhao, *J Am Chem Soc*, 2019, **141**, 1141-1149.
2. G. Kresse and J. Hafner, *Phys. Rev. B* 1994, **49**, 14251-14269.
3. G. Kresse and J. Hafner, *Phys. Rev. B*, 1993, **47**, 558-561.
4. G. Kresse and J. Furthmüller, *Comput. Mater. Sci.*, 1996, **6**, 15-50.
5. G. Kresse and J. Hafner, *J. Phys. Condens. Matter*, 1994, **6**, 8245-8257.
6. G. Kresse and J. Furthmüller, *Phys. Rev. B*, 1996, **54**, 11169-11186.
7. G. Kresse and D. Joubert, *Phys. Rev. B*, 1999, **59**, 1758-1775.
8. J. P. Perdew, K. Burke and M. Ernzerhof, *Phys. Rev. Lett.*, 1996, **77**, 3865-3868.
9. W. Setyawan and S. Curtarolo, *Comput. Mater. Sci.*, 2010, **49**, 299-312.
10. J. Callaway and H. C. von Baeyer, *Phys Rev*, 1960, **120**, 1149-1154.
11. J. Callaway, *Phys Rev*, 1959, **113**, 1046-1051.
12. M. Hong, Z. G. Chen, L. Yang, Y. C. Zou, M. S. Dargusch, H. Wang and J. Zou, *Adv Mater*, 2018, **30**.
13. Y. Jiang, J. Dong, H.-L. Zhuang, J. Yu, B. Su, H. Li, J. Pei, F.-H. Sun, M. Zhou, H. Hu, J.-W. Li, Z. Han, B.-P. Zhang, T. Mori and J.-F. Li, *Nat. Commun.*, 2022, **13**.